Microsyst Technol
DOI 10.1007/s00542-016-2817-3

TECHNICAL PAPER

Development of a biomimetic underwater microrobot for a father–son robot system

Maoxun Li[1] · Shuxiang Guo[2,3] · Jin Guo[2] · Hideyuki Hirata[2] · Hidenori Ishihara[2]

Received: 25 August 2015 / Accepted: 6 January 2016

Abstract Conventional underwater intervention tasks are performed by underwater vehicles equipped with rigid multi-link arms. However, the movements of conventional mechanical arms exert reactive force on the vehicle platform due to their enormous bulk. Additionally, they cannot be used for small object recovery. In this paper, an ionic conducting polymer film (ICPF) actuator-based crayfish-inspired microrobot is designed and developed as a son robot for object recovery, which is connected to the amphibious father robot by copper wires. The crayfish-like son robot is used as the mechanical arm of the father–son robot system, which can grasp the small object especially in restricted spaces. The crayfish-inspired son robot actuated by ten ICPF actuators can realize underwater basic motions. The father robot can emit the son robot for object recovery. A proximity sensor is mounted in front of the microrobot between the two ICPF hands to implement the autonomous grasping motion. And we designed a blue LED-based underwater optical communication system to realize the communication between the father robot and the son robot for microrobot recovery. We carried out the experiments to confirm the basic operations of the microrobot, evaluate the performance of the communication system, and verify the blue LED tracking mechanism for microrobot recovery.

✉ Jin Guo
guojin0522@gmail.com

Maoxun Li
s14d505@stmail.eng.kagawa-u.ac.jp

1 Graduate School of Engineering, Kagawa University, Hayashichou, Kagawa 2217-20, Japan

2 Faculty of Engineering, Kagawa University, Hayashichou, Kagawa 2217-20, Japan

3 Key Laboratory of Convergence Medical Engineering System and Healthcare Technology, The Ministry of Industry and Information Technology, School of Life Science, Beijing Institute of Technology, No. 5, Zhongguancun South Street, Haidian District, Beijing 100081, China

1 Introduction

Underwater vehicles have been extensively applied to underwater intervention missions instead of human in recent years. As the crucial equipment of underwater vehicles, underwater manipulators typically play an important role in the underwater tasks. Generally, underwater manipulators are operated manually by human with remotely operated vehicles (ROVs). A KORDI ROV with a dual teleoperated manipulator was designed and developed (Jun et al. 2008). The ORION manipulator has six functional joints and one gripper. However, a ROV equipped with a rigid multi-link arm requires a depot ship for operations and the tether connected to the depot ship also restricts its positioning and manipulation performance.

On the contrary, autonomous underwater vehicles (AUVs) do not require the depot ship and the tether. Thus, AUVs can achieve a better positioning performance and a higher flexibility than ROVs. Nowadays, only few AUVs are equipped with underwater manipulators. SAUVIM, capable of autonomous manipulation, performed an autonomous underwater intervention in the oceanic environment (Marani et al. 2009). And it completed an underwater recovery mission, which includes searching for the target and bringing it back to the surface. In addition, an underwater vehicle-manipulator system was used on an underwater robot with six degrees of freedom (DOF) (Mohan and Kim 2012, 2015). A 3-DOF underwater manipulator was mounted on the robot for underwater intervention. RAUVI,

Published online: 14 January 2016

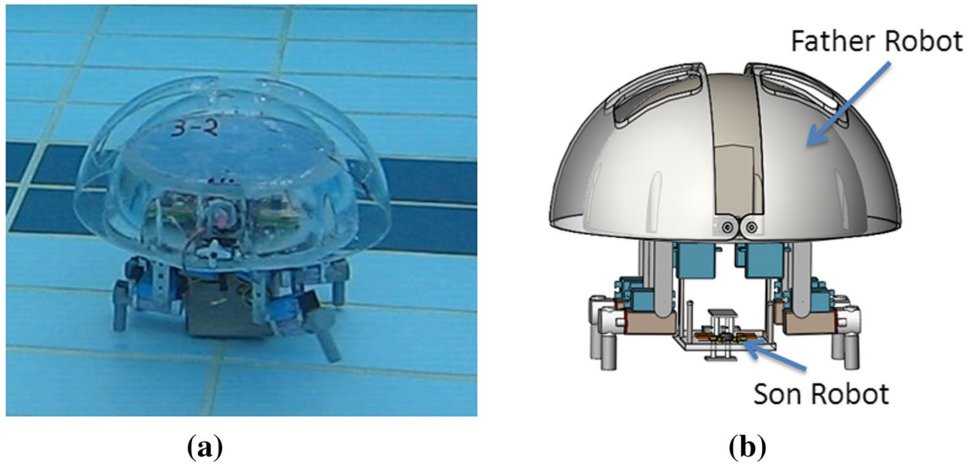

Fig. 1 Father–son robot configuration: **a** prototype of the amphibious father robot and **b** the conceptual design of the father–son robot system

a reconfigurable AUV, was designed and developed for intervention, which was equipped with acoustic and optic sensors for environmental perception and a robotic arm for simple tasks (De Novi et al. 2009). These researches are relying on the multi-link arm to implement underwater missions (Antonelli et al. 2001; Cui and Sarkar 2000). As a conventional manipulation system, the multi-link arm is appropriate for heavy-type work and continuous manipulation.

However, conventional underwater mechanical arms are commonly enormous and they are mounted on a free floating vehicle platform for recovering large-sized objects. The weightlessness of a vehicle underwater is similar to that in space. During the underwater manipulation tasks, the underwater vehicle has to overcome the reaction from the mechanical arm in order to keep it in its position. Furthermore, considering the nonlinear and hydrodynamic coupling between the underwater vehicle and the mechanical arm, developing a control scheme is required to compensate for the movement of the vehicle induced by the movement of the arm, which increases the complexity of the control system.

To overcome these difficulties, some researchers begin to use a small, deployable and highly maneuverable ROV as the manipulator. A novel manipulation system concept was proposed for AUVs. An agent vehicle, as a manipulator, was developed to be connected to a main AUV by a smart cable to implement underwater manipulations, which is very useful for the target not on the seabed (Yu et al. 2013). As the size of the agent is slightly large, it is not suitable for the small-sized AUV. In our lab, a microrobot was designed as a grasper of FURIS to be connected to a small-sized AUV for underwater missions (Yue et al. 2015). But since the microrobot can only realize the grasping motion, it is hard for the AUV to detect the target and control the microrobot to move to the position directly above the target. For these AUVs, performing the underwater tasks in restricted and complicated environments is more difficult.

To solve the above-mentioned limitations, we proposed a father–son robot system which employed a microrobot as the mechanical arm for small object recovery. In our previous research, a small amphibious spherical robot was designed and developed (Li et al. 2015). Generally, underwater vehicles need to be shipped to the operation waters and recycled after underwater tasks. Compared with underwater robots, amphibious robots can walk from the ground to the water without shipping, and vice versa (Dudek et al. 2007; Zhang et al. 2013). Moreover, symmetry of the spherical shape provides superiority of flexibility and no dynamic coupling (Chase and Pandya 2012; Lin et al. 2010). And a sphere provides high compression resistance as well. The conceptual design of the father–son robot system is shown in Fig. 1. For carrying and deploying the microrobots, we developed a fixture mechanism installed on lower hemisphere of the amphibious robot. In order to simplify the control system, this mechanism was designed with no actuating parts, as shown in Fig. 2.

When designing the microrobot, several constraints must be taken into account. First, as the holder on the amphibious robot for carrying microrobots has a finite size, the microrobot should be designed to be miniaturization. Second, since the father robot is a small-sized AUV, it cannot provide too high energy for itself and the microrobots. Thus, the low-powered actuators are required for driving microrobots. Finally, in view of the implementation of the low power consumption, the microrobot should be light in weight.

According to the above restrictions, smart material-based microrobots are appropriate to be the mechanical arms of the father–son robot system. In contrast to conventional actuators, smart materials, like ionic conducting polymer film (ICPF), shape memory alloy (SMA), piezoelectric elements, and pneumatic actuator etc., can be employed as actuators directly and it is easy for them to realize the flexible movements with the advantages of small size and

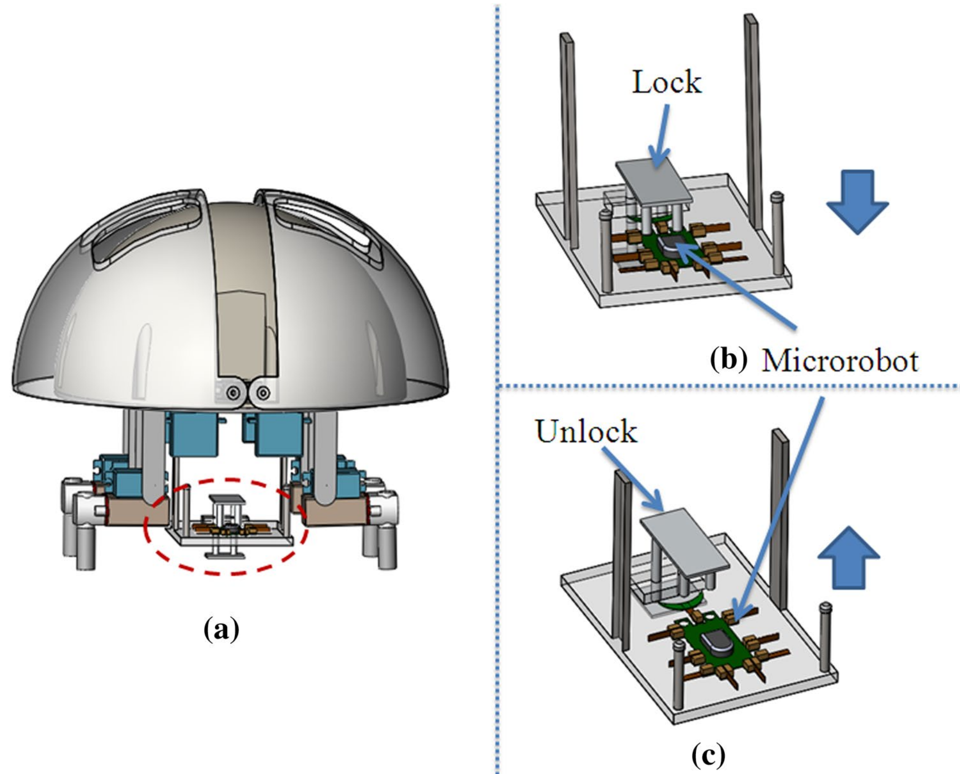

Fig. 2 Fixture mechanism of the microrobot: **a** father–son robot system, **b** microrobot in locked state and **c** microrobot in free state

light weight (Kim 2011; Chen et al. 2010; Yeom et al. 2009; Shi et al. 2012; Gao et al. 2011). Compared with other smart materials, ICPF actuators have the advantages of compact structure, low driving voltage, and low noise, ability of driving in water, soft characteristic, and quick response properties. Therefore, ICPF actuators are more suitable to drive the son robot of the father–son robot system. As swimming motion cannot realize a comparatively precise position control, designing a legged robot as the son robot is an excellent option for underwater tasks.

Accordingly, to implement the underwater intervention, we described a father–son robot configuration, which is consisted of an amphibious spherical father robot and an ICPF-actuated legged microrobot. The father robot with a high mobile velocity provides the power and sends control signals to the microrobot, as shown in Fig. 1. The purpose of this paper is to design a son robot to realize the object recovery and tracking mechanism. After the underwater mission, the son robot can get back to the father robot with the target object.

This paper is organized as follows. In Sect. 2, we described the design of the son robot, including the actuators, the structure design, power supply and the locomotion mechanisms. Then we did the performance evaluation of ICPF actuator, photodiode and proximity sensor in Sect. 3. Section 4 introduced the prototype microrobot and the underwater experiments. Finally, we drew the conclusions in Sect. 5.

2 Design of son robot

2.1 ICPF actuators

Compared with other actuators, ICPF actuators are capable of the work in both air and water. As an innovative material, ICPF is made of an ionic polymer membrane Nafion 117 chemically plated with gold electrodes on both sides. Owing to the change of the chemical structure of ICPF, a bending deformation will occur when an external electric stimulus is applied across it.

In view of this phenomenon, ICPF can be used as an actuator. When voltage is applied across both electrodes of ICPF, it will bend towards the positive electrode. Consequently, we used Nafion 117 to process and fabricate the ICPF for our research. The most common shape of ICPF actuator is rectangle, which can generate a stable deflection and bending force (Abdelnour et al. 2012).

ICPF actuators have the characteristics of soft and compact structure, quick response, and low drive voltage, low noise. What's more important is that ICPF is capable of driving in water. With these advantages, ICPF actuators are appropriate to drive the son robot for the father–son robot system. Due to its property of quick response, ICPF actuators are used as undulating and oscillating fins for fish-like microrobots (Gao and Guo 2010; Chen et al. 2010). However, swimming motion actuated by undulating and

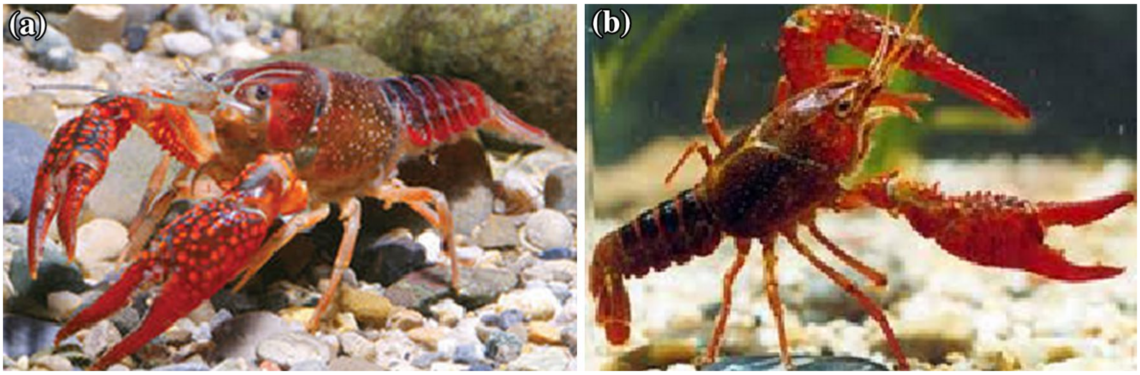

Fig. 3 The crayfish in **a** walking motion and **b** grasping motion

oscillating fins cannot ensure a precise position control of the robot. Also a fish-like robot cannot use the fins to realize a backward motion. To design a legged robot as the son robot is required for underwater missions.

2.2 General design of son robot

Nature provides many perfect models for robots. And many researchers did research on the biomimetic robots. For the crayfish, it has eight legs and two claws. The crayfish can walk underwater and grasp objects with its two big claws. Thus, we design a son robot which is inspired by the crayfish. Figure 3 shows a crayfish in walking and grasping motions.

To design a son robot, we should consider several constraints including the finite size of the holder on the father robot and limited power supply provided by father robot. Hence, the son robot is designed with the characteristics of miniaturization, light weight, low power consumption and driven by smart actuators. An eight-legged crayfish-like underwater microrobot is proposed to be the son robot of the father–son robot system. This microrobot is composed of a main body, ten ICPF actuators, eight of which are legs for driving the robot and others are hands used as a claw for grasping objects, and several wires connected to the father body for receiving the control signals and power supply. Four legs are used as the drivers to drive the robot to implement a two-DOF movement. And others are used as supporters to lift the robot up. Considering the size of the holder, the size of the body of the robot are determined to be 24 mm long, 24 mm wide and 3.5 mm high and the size of the ICPF actuators are all determined to be 17 mm long, 3 mm wide and 0.2 mm thick. Each ICPF actuator has one degree of freedom. The conceptual design of the microrobot is shown in Fig. 4.

Two photodiodes, the light sensors, are mounted in front of the robot to implement the tracking motion, including tracking the target object and other microrobots, especially

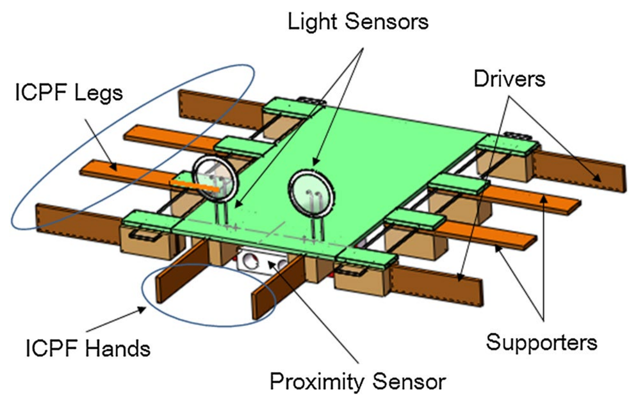

Fig. 4 Conceptual design of the crayfish-like microrobot

tracking the father robot. With the tracking mechanism, the microrobot is able to get back to the father robot. Besides, an infrared proximity sensor is mounted on the bottom of the robot. Set the sensor between the two hands to detect the target object for object recovery.

2.3 Electrical system and power supply

The control center of the father robot is based on an AVR ATMEGA2560 micro-controller, which is also the control center of the son robot. The control system of the father–son robot system is shown in Fig. 5. The micro-controller uses eight input/output ports to control ten ICPF actuators. One ICPF actuator is controlled by two input/output ports. We utilized three data transmission ports and analog-to-digital conversion; therefore, the microcontroller could receive and transmit data to control the photodiodes and the infrared proximity sensor, thereby implementing closed-loop control.

Four batteries are used as the power supply: two 6TNH22A/8.4 V batteries to provide power to the AVR micro-controller and ICPF actuators, and two

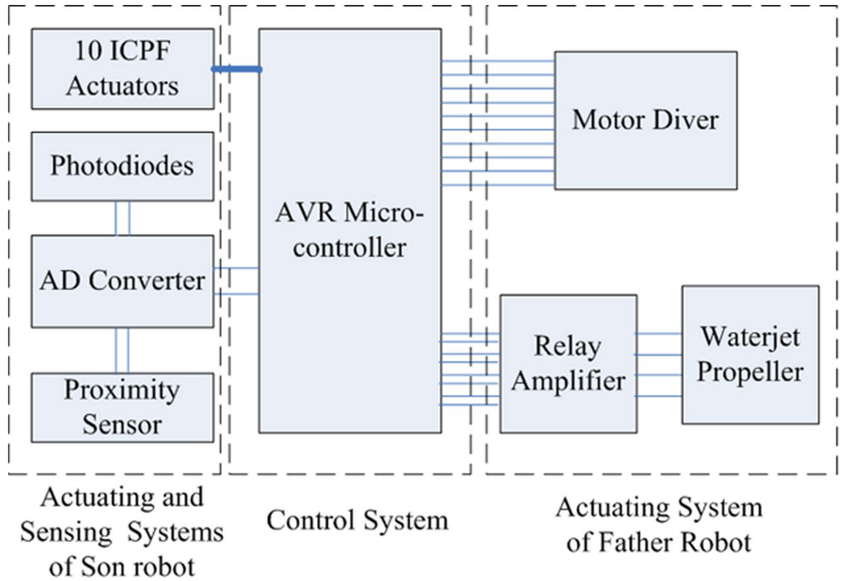

Fig. 5 Control system of the father–son robot system

YBP216BE/7.4 V batteries to provide power to four waterjet propellers and ten servomotors.

2.4 Walking and rotating mechanisms

The crayfish-like microrobot employs eight legs to implement walking and rotating motions. The microrobot can realize each step cycle of walking forward motion with the following four steps, as shown in Fig. 6. First, four supporters bend downwards to lift the body of the robot up, and now the drivers are kept off the ground. Second, when the body is lifted by the supporters, the four drivers off the ground bend forward. Thirdly, the supporters bend upwards so that they do not connect with the ground, and now the drivers are on the ground to support the body. Finally, the four drivers bend backward to generate the friction to make the robot move forward. The drivers are adopted to drive the robot and the supporters are to reduce the resistance from the ground. The oscillating frequencies of drivers and supporters are set to the same value, and the phase of the supporters is set to a value lagging behind that of the drivers by 90°. When the drivers on different sides bend towards different directions, the microrobot can implement the rotating motion, as shown in Fig. 6. According to the above, a series of walking and rotating motions can be performed, including walking forward/backward, rotating clockwise/counterclockwise.

Assuming that the tip displacement of ICPF actuator is equal to $d/2$, we can achieve an average speed by (1).

$$v = d \times f \tag{1}$$

where v is the average speed, d means the distance that the robot advances per step cycle and f is the control frequency.

2.5 Grasping mechanism

Two ICPF actuators as the hands of the microrobot are used to imitate a pair of claws of a real crayfish. The mechanism of the grasping motion is shown in Fig. 7. When the cathode of power supply is connected to the inner sides of the ICPF actuators, the ICPF hands bend outwards, which is in the open state. When the anode of power supply is connected to the inner sides of the ICPF actuators, the ICPF hands bend inwards, which is in the closed state. Two hands are fastened to the front of the microrobot with a distance of approximately 10 mm. The bending force generated by the two ICPF hands is determined by the driving voltage and the tip displacement. At a given voltage, with the deflection increasing, the bending force decreases. Consequently, the size of the target object determines the performance of the grasping motion.

3 Performance evaluations

3.1 ICPF actuators

Considering the compact structure of the son robot, the size of the ICPF actuators are all determined to be 17 mm long, 3 mm wide and 0.2 mm thick. As the performance of ICPF is depending on the effectiveness of fabrication processing, before mounting the ten ICPF actuators on the microrobot, we measured the tip deflection of a single ICPF actuator under different control frequencies for its performance evaluation. Figure 8 shows the experimental setup of deflection measurement for an ICPF actuator. The actuator is driven by a series of external control signals to bend in two directions recurrently. The tip deflection of the ICPF

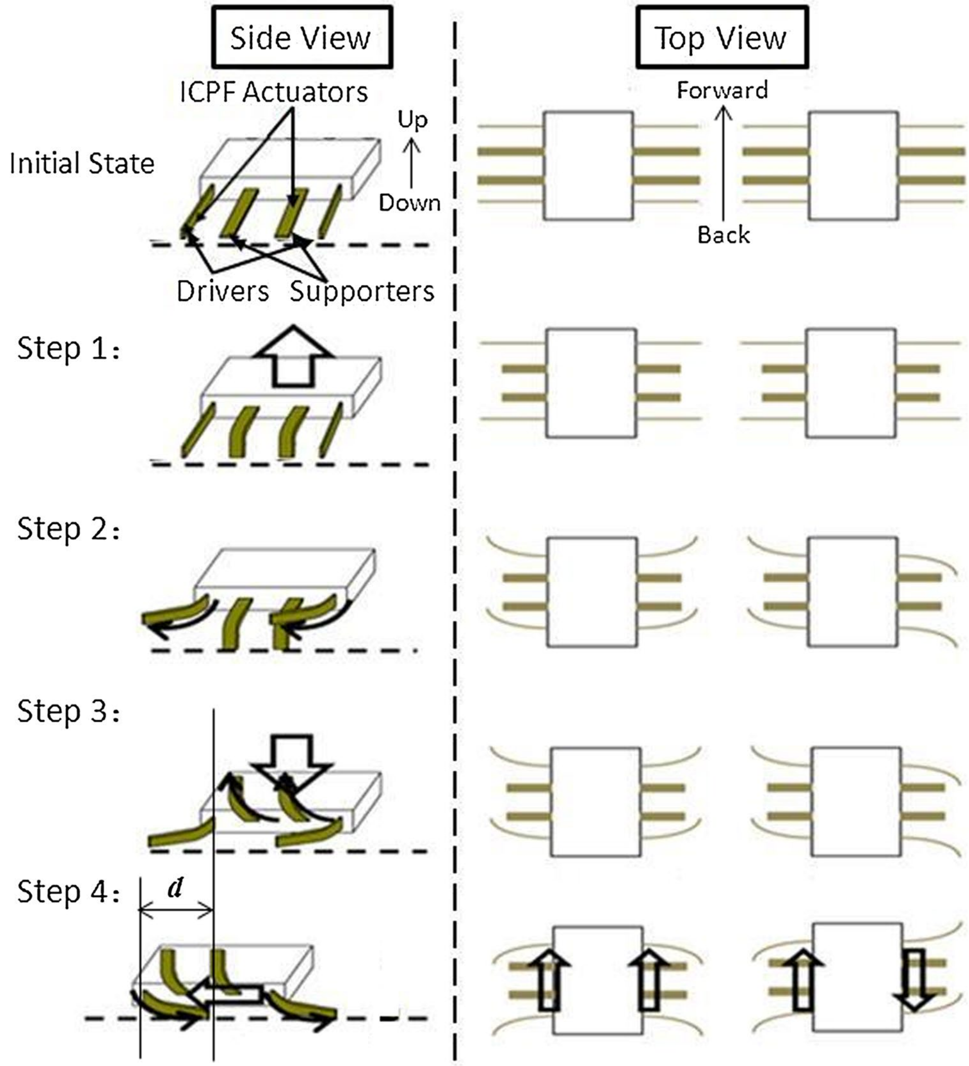

Fig. 6 One step cycle of moving forward and rotating clockwise motions

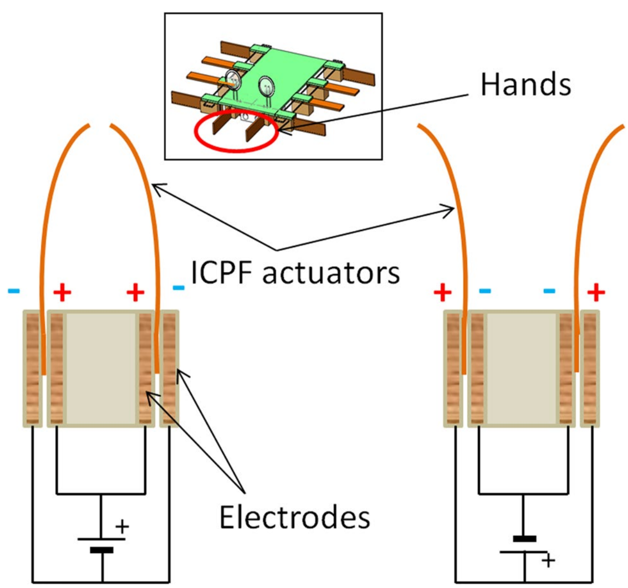

Fig. 7 Mechanism of the grasping motion

actuator is measured by a laser sensor, which can convert the distance to a voltage automatically. The laser sensor is connected to a personal computer (PC) with an analog–digital conversion (ADC). Through the relationship between the measured voltage and the distance, the tip displacement is calculated by the PC. The sample of ICPF actuator is 17 mm long, 3 mm wide and 0.2 mm thick.

During the experiments of the tip deflection measurement, two given voltages of 4 and 6 V are applied to one end of an ICPF actuator respectively. These experiments are conducted under a control frequency of 1 Hz. We used the laser sensor to measure the change of the tip displacement over time. The results of the change of the tip reflection are shown in Fig. 9. Then, we changed the control frequency from 0.5 to 7 Hz and measured the tip displacement under different frequencies. The experiments under each control signal are repeated 5 times to achieve an average tip displacement. The experimental results are shown in Fig. 10. From the results, the tip displacement decreases as

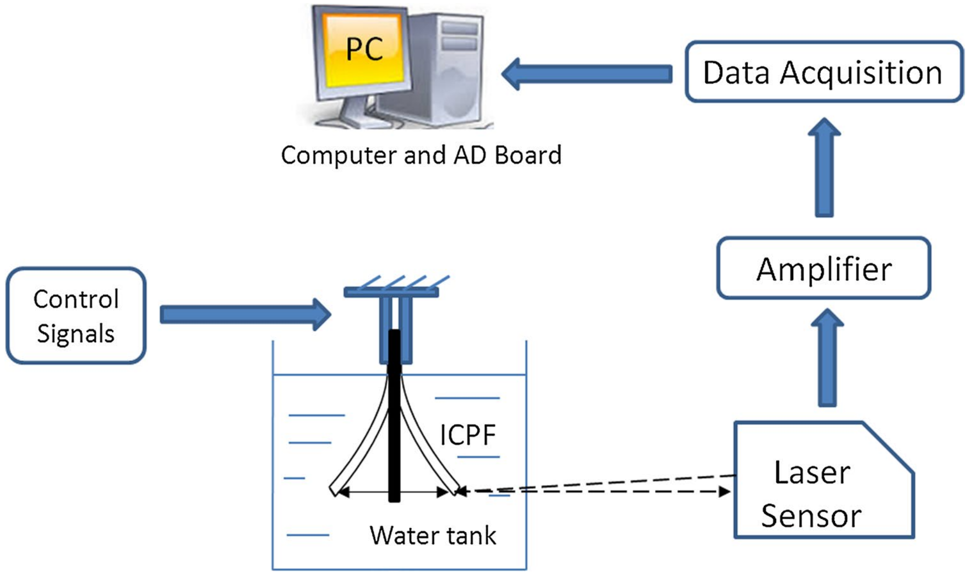

Fig. 8 The experimental setup of deflection measurement for an ICPF actuator

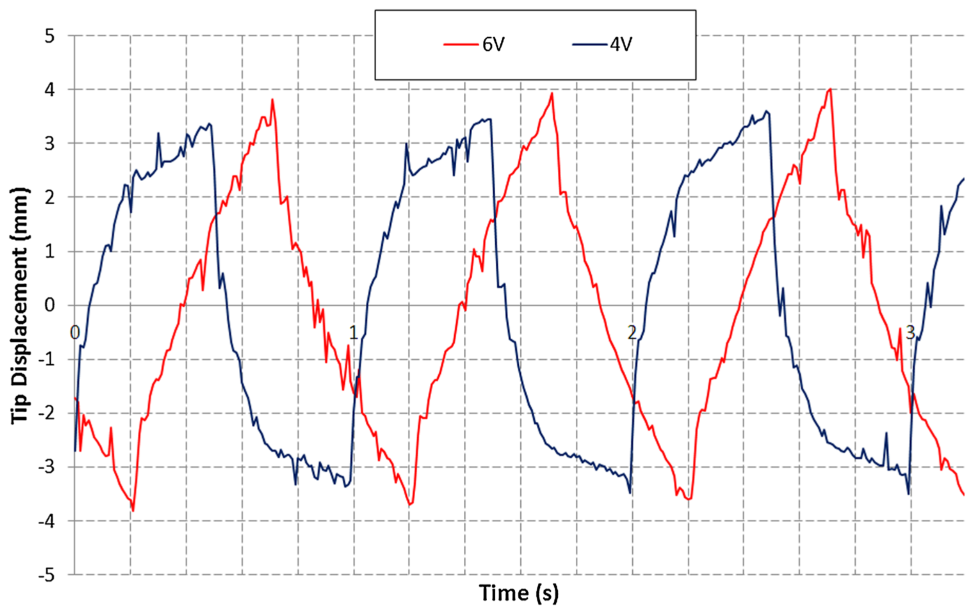

Fig. 9 Experimental results of deflection measurement for ICPF actuator with time

the control frequency increases. At relatively high voltages, the tip displacement decreases rapidly as a function of frequency. According to the Eq. (1), we know that with the frequency increasing, the average speed will increase first and then decrease to zero.

3.2 Blue LED and photodiodes

Nowadays, there are several kinds of communication methods, including radio communication, acoustic communication and optical communication. However, underwater robots cannot employ radio frequency signal for communication as its high attenuation underwater. As an established technology, acoustic underwater communication typically requires high power and high cost, and delivers low data rates, and is used for relatively large devices. Therefore, it is difficult for small underwater robots to use it. And optical communication becomes a compact, high-data rate and inexpensive alternative, which is used for short-to-median distance communication (Tian et al. 2013; Brundage 2010; Cox et al. 2008). Compared with laser-based communication systems, LED-based communication systems with the characteristics of low cost, small size and no stringent requirement on directionality are appropriate for small-sized underwater robots. And the light attenuation of blue light is less than that of others in clear water.

Consequently, in order to realize the communication among the father robot and several son robots, we designed

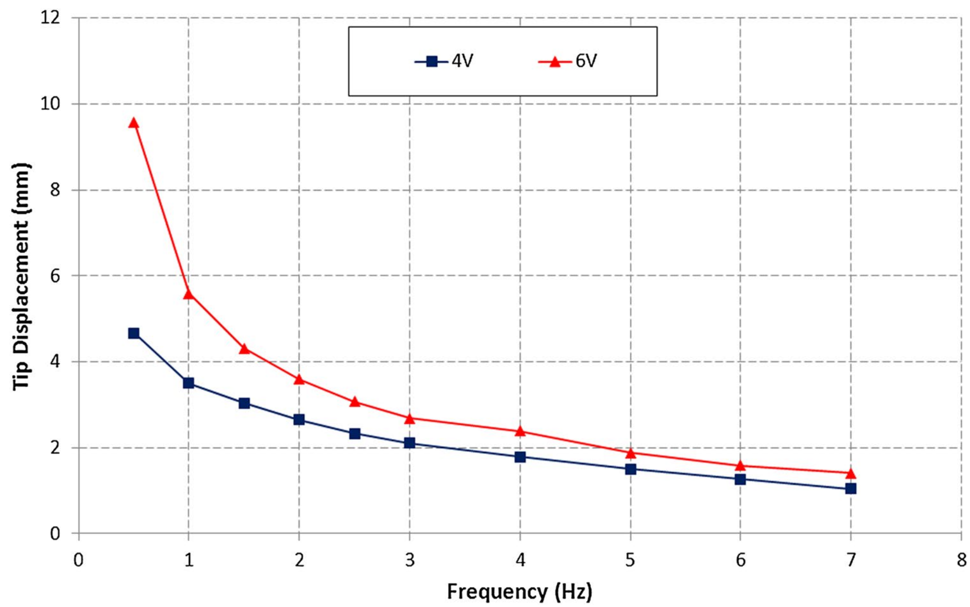

Fig. 10 Experimental results of deflection measurement for ICPF actuator under different control frequencies

a blue LED-based underwater optical communication system, including the transmitter, the receiver and an agreed communication protocol between them. In our design, the super blue LED is applied as the transmitter and the photodiode is used as the receiver. The receiver on the robot can capture the light signal which is emitted by the transmitter. The blue LED is sealed in a plastic bag for waterproof. To implement high efficiency and low cost underwater, an Advanced Photonix PDB-V107E with the advantages of high response and low noise is employed as the light sensor, which is a blue enhanced photodiode and enlarges the sensitivity of blue light.

We evaluated the performance of the communication system before equipping the light sensors on the microrobot. A photodiode and a blue LED constitute a optical coupler. The experiments are conducted in a huge water tank. In order to avoid interference generated by other light sources, during the whole experiments only the blue LED can be lighted on. The experimental setup of the communication system is placed in a water tank including a blue LED and a photodiode, as shown in Fig. 11a. When the center of the photodiode and the center of the blue LED are in a straight line, we set the input angle of blue LED to 0°, as shown in Fig. 11b. We measured the signal strength detected by the photodiode under different input angles and different transmission distances for the communication performance test.

Three kinds of communication experiments are carried out. The first one is to detect the variation of the signal strength under a fixed input angle of 0° and different transmission distances. In this experiment, we place a blue LED in a fixed position in the water tank and place the

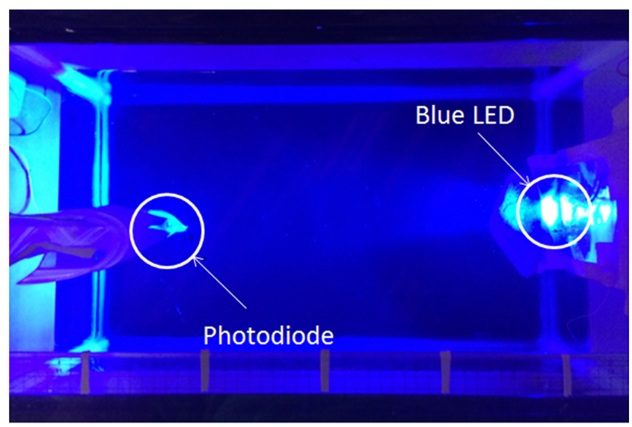

(a)

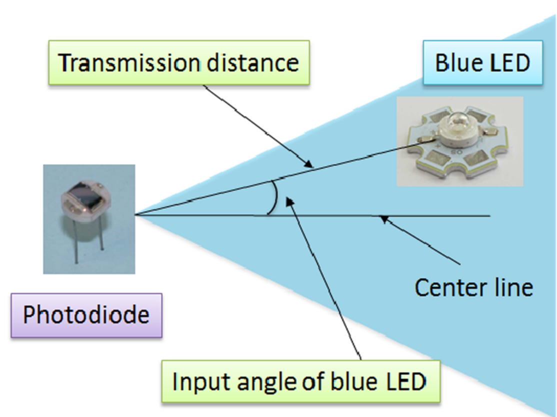

(b)

Fig. 11 **a** The experimental setup for performance evaluation of communication system in a water tank and **b** illustration of experimental variables

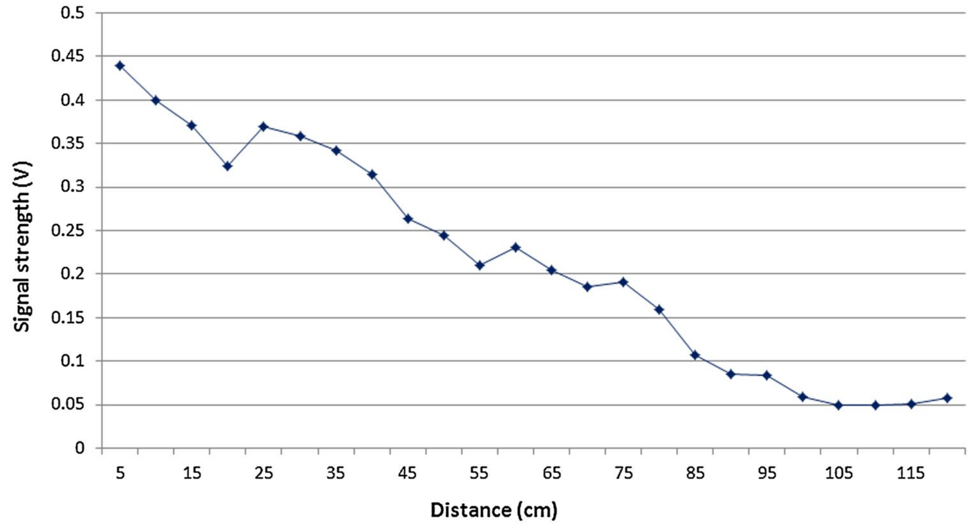

Fig. 12 Experimental results of signal strength at different transmission distances

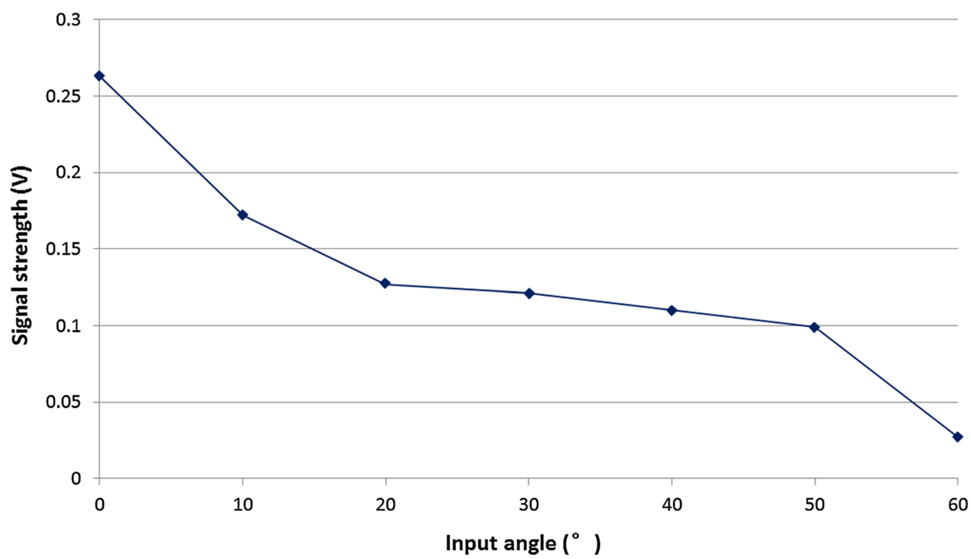

Fig. 13 Experimental results of signal strength under different input angles at a distance of 45 cm

photodiode from the transmitter at 24 different distances. We used the photodiode to measure the signal strength at intervals of 5 cm. Figure 12 shows the experimental results of signal strength at different transmission distances. From the results, the detected signal strength declines as the distance between the transmitter and the receiver increases. The communication system can be applied at a maximum transmission distance of 120 cm, which is enough for the communication between the father robot and the son robot.

The second experiment is conducted to detect the variation of the signal strength under different input angles at a fixed distance of 45 cm. The photodiode is placed in a fixed position in the water tank and the blue LED is placed from the receiver at a constant distance of 45 cm with different input angles in the angular range from 0° to 60°. The experimental results of the signal strength under different input angles are shown in Fig. 13. As the input angle of the blue LED increases from 0° to 60°, the signal strength detected by the photodiode decreases. When the input angle is set over 60°, the photodiode cannot detect any signal strength. Therefore, the photodiode shows a better performance when it is placed from the blue LED at a distance of 120 cm and at an input angle of 0°.

The third experiment is to measure the detectable range of the photodiode in the coverage area of the blue LED, as shown in Fig. 11b. We measured the detectable maximum distance of the photodiode at different input angles in the angular range from −60° to 60°. As the signal strength detected by the photodiode <0.05 V cannot enable the communication, the maximum distances with a measured signal strength over 0.05 V at different input angles constitute the detectable range of the communication system. We recorded the maximum transmission distances at intervals of 10°. The experimental results of the detectable range are

Fig. 14 Detectable range of the communication system

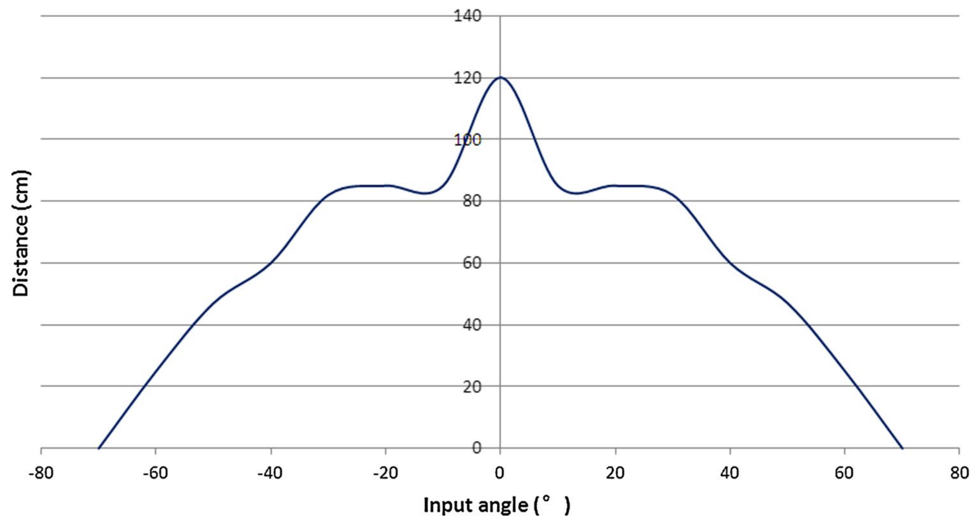

shown in Fig. 14. From the graph, with the increasing input angle, the detectable range of the system declines. Within this range, the light sensor can detect the signal strength emitted by the blue light source well.

3.3 Proximity sensor

To implement the autonomous grasp for the microrobot, a proximity sensor is mounted in front of the robot right below the photodiodes. The sensor is set between the two hands to imitate the eye of the crayfish to detect the distance between the target object and the microrobot. The dimensions of the infrared proximity sensor used on the robot are 10×5 mm with a weight of around 0.7 g. With an angle measurement range from $-30°$ to $30°$, the proximity sensor can detect the total space between two ICPF hands.

We calibrated the proximity sensor to measure the distance between the sensor and the target object. The calibration results indicate the relationship between the distance and the detected voltage. During the experiments, we changed the distance gradually from 60 to 25 mm and measured the output voltage increasing slowly from 0 to 0.2 V. However when the distance is <25 mm, the output voltage increased rapidly. Depending on the measured voltages, the microrobot is able to know the remaining distance to the target object. According to the distance, the microrobot can control the ICPF hands to be open and closed to catch the object.

4 Prototype microrobot and experiments

4.1 Prototype microrobot

In order to implement the underwater missions, we proposed a crayfish-like underwater microrobot which is mounted on the father robot for object recovery and

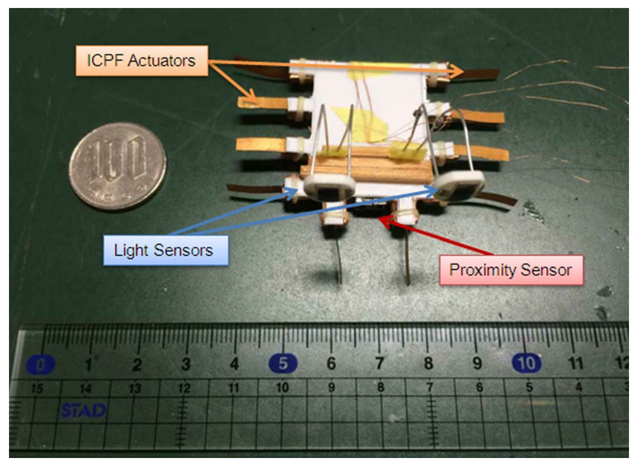

Fig. 15 The prototype microrobot

tracking. An eight-legged crayfish-inspired microrobot, as the son robot of the father–son robot system, is constructed, as shown in Fig. 15. Eight ICPF actuators are employed to actuate the microrobot and two ICPF actuators in front of the robot are used to mimic the claw of the crayfish for grasping object. Each ICPF actuator is connected to the plastic body of the robot with a rubber band. The father robot controls the microrobot by a kind of enamel covered copper wires with a diameter of 0.03 mm. The resistance of the wires could be ignored by the reason of its high flexibility. The dimensions of the microrobot are $24 \times 24 \times 3.5$ mm. The dimensions of ICPF actuators are $17 \times 3 \times 0.2$ mm.

4.2 Walking/rotating experiments in a water tank

Walking and rotating motions are two basic motions for the microrobot. To evaluate the performance of the basic

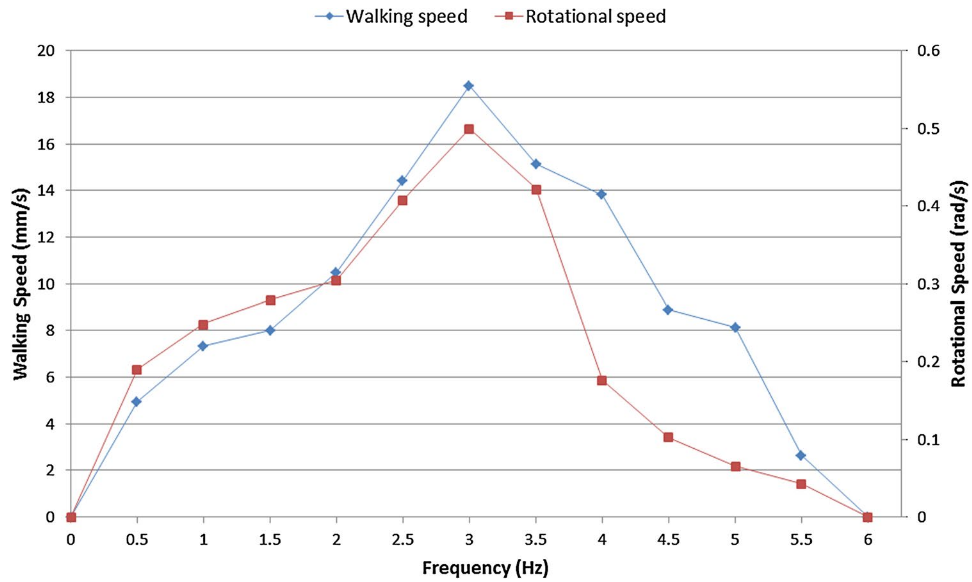

Fig. 16 Experimental results for the microrobot

motions of the robot, walking and rotating experiments were conducted in a water tank at a given control voltage of 8 V. The microrobot is connected to the control circuit with several copper wires. During the walking and rotating experiments, we changed the applied frequencies and calculated the walking and rotational speeds of the microrobot at each control frequency separately by recording its running time. To achieve an average speed, all experiments were repeated 5 times at a set of control signals.

The experimental results of walking and rotational speeds are shown in Fig. 16. From the results, we achieved a maximum walking speed of 18.6 mm/s and a maximum rotational speed of 0.51 rad/s at a control frequency of 3 Hz. The walking speed of the robot is related to the step size and the control frequency. From our previous research results, we know that the step size is in inverse proportion to the applied frequency. Therefore, with the control frequency increasing, the average walking speed will increase at first and then decrease to zero. So does the rotational speed.

4.3 Grasping experiments

To implement the autonomous underwater object recovery, an infrared proximity sensor was mounted on the robot between the two ICPF hands, as shown in Fig. 15. The dimensions of the sensor is 10×5 mm and the weight of it is 0.7 g. As we mentioned in Sect. 3, the measurable distance range of the sensor is from 0 to 6 cm and the detectable output voltage is from 200 mV to the power voltage. During the experiments, the robot was programmed to move along the configured path. When the microrobot gets close to the target object, the micro-controller mounted on the father robot will receive data from the proximity sensor and then judge the realtime distance to the target. According to the detected distance, the robot will open the ICPF hands at a distance of over 20 mm to the target and then close them to grasp the object when the distance to the target is <10 mm.

We carried out the grasping experiments to evaluate its performance. At first, the robot was controlled to move along a pre-setting route. When the proximity sensor carried on the robot detected the target around 20 mm away, the robot began to open their hands. The ICPF hands were kept open until the target was detected around 10 mm away from the proximity sensor. At a distance of 10 mm from the target, the robot closed the ICPF hands to grasp the object. Then the robot carried the target object to the desired location.

4.4 LED-based tracking experiments

For the father–son robot system, the father robot should recover the microrobot with the target object after the son robot finished the underwater tasks. In order to realize the microrobot recovery, a blue LED-based underwater optical communication system is designed for the father–son robot system. A super blue LED is installed on the shelf of the lower hemisphere of the father robot, which is used as the transmitter of the optical communication system. And two light sensors, which are used as the receivers, are mounted in front of the microrobot symmetrically, as shown in Fig. 15. The two receivers on the microrobot can capture the light signal emitted by the transmitter.

By comparing the strength of light signal received by the two light sensors, the microrobot is able to change its motion among walking straight, turning left and turning right motions. According to the results of the performance

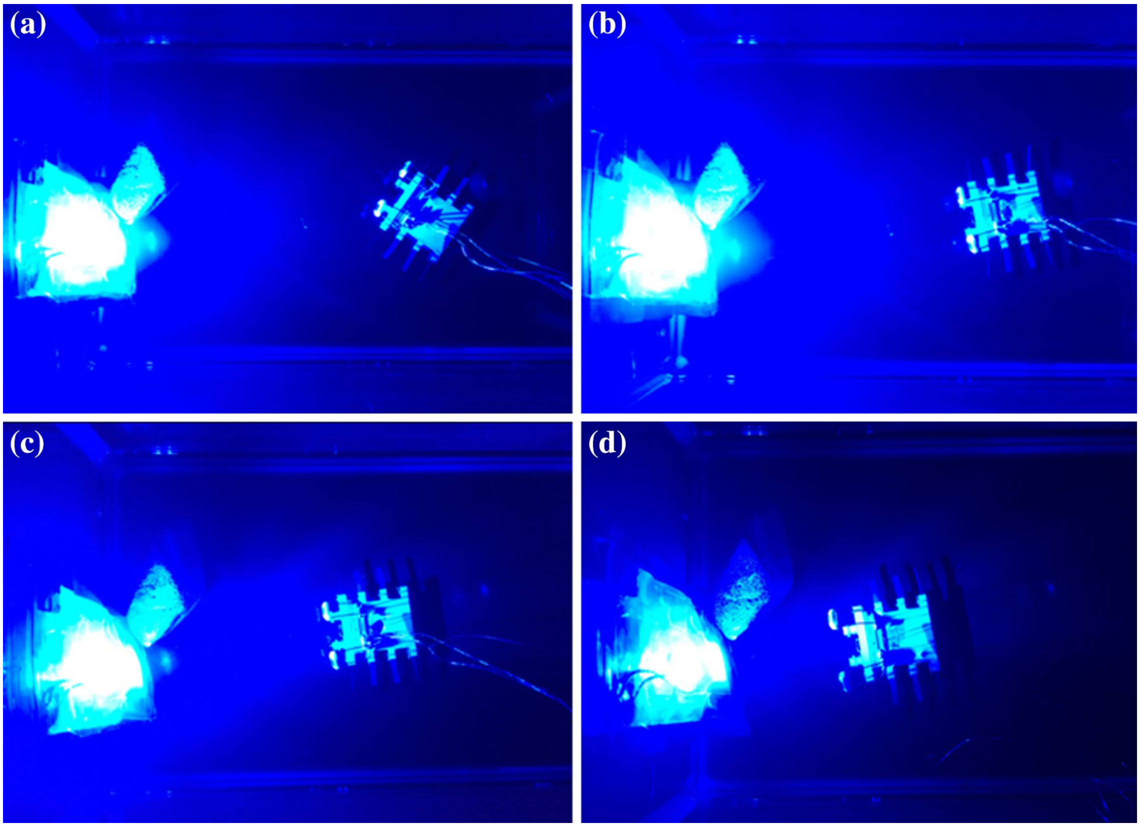

Fig. 17 Blue LED tracking experiments

evaluation of the blue LED-based underwater optical communication system, a threshold value was set previously for the motion control of the microrobot. When the difference of the signal strength captured by two light sensors is larger than the threshold value, the microrobot will implement rotating motion. On the contrary, the microrobot will walk straight. When the signal strength captured by the photodiode on the left is larger than that captured by the photodiode on the right, the microrobot will turn left, whereas, the microrobot will turn right. Thus, the microrobot can walk to the LED automatically with the underwater optical communication system. We conducted the blue LED tracking experiments in a water tank, as shown in Fig. 17. To avoid interference generated by other light sources during the whole experiments, only the blue LED is lighted on. During the experiments, the microrobot turned left until it faced to the blue LED, and then moved to the LED straightly. From the experimental results, we know that the son robot can realize the blue LED tracking motion underwater.

Thus, the microrobot will track the blue LED carried on the bottom of the father robot for son robot recovery. With the function of tracking the blue LED, the microrobot can get back to the father robot.

5 Conclusion

In this paper, a crayfish-like son robot for the father–son robot system has been developed. The son robot is an ICPF actuator-based microrobot. The crayfish-inspired son robot is adopted as the mechanical arm of the father–son robot system. The son robot is actuated by ten ICPF actuators, which can perform walking, rotating and grasping motions underwater. A proximity sensor and two photodiodes are mounted in front of the microrobot to implement the functions of autonomous grasp and blue LED tracking. A blue LED-based underwater optical communication system is designed to enable the communication between father robot and son robot for microrobot recovery.

The walking, rotating and grasping experiments are conducted to verify the performance of the basic motions of the robot. From the experimental results, a maximum walking speed of 18.6 mm/s and a maximum rotational speed of 0.51 rad/s are achieved at a control frequency of 3 Hz. We also carry out the underwater experiments to evaluate the performance of the optical communication system, in which the blue LED and the photodiode are used as the transmitter and the receiver respectively. From the results, the photodiode can detect the blue LED at a maximum distance of 120 cm. By measuring the detectable maximum distance of the photodiode at different input angles, we achieve the detectable range of the communication system. Finally, we carry the light sensors on the microrobot and conduct the grasping experiments and the blue LED-based tracking experiments. From the results, the robot can realize the functions of object recovery and LED tracking motion underwater.

With the function of tracking blue LED, the wireless underwater communication among the father robot and several son robots can be implemented. In the future, we consider designing a new wireless microrobot used as the mechanical arm of the father–son robot system. Using the wireless communication method, son robots can communicate with each other and also communicate with the father robot.

Acknowledgments This research is partly supported by National Natural Science Foundation of China (61375094), Key Research Program of the Natural Science Foundation of Tianjin (13JCZDJC26200), National High Tech. Research and Development Program of China (No. 2015AA043202), and SPS KAKENHI Grant Number 15K2120.

References

Abdelnour K, Stinchcombe A, Porfiri M, Zhang J, Childress S (2012) Wireless powering of ionic polymer metal composites toward hovering microswimmers. IEEE/ASME Trans Mechatron 17:924–935

Antonelli G, Chiaverini S, Sarkar N (2001) External force control for underwater vehicle–manipulator systems. IEEE Trans Robot Autom 17:931–938

Brundage H (2010) Designing a wireless underwater optical communication system. Master's thesis, Massachusetts Institute of Technology, Cambridge, MA

Chase R, Pandya A (2012) A review of active mechanical driving principles of spherical robots. Robotics 1(1):3–23. doi:10.3390/robotics1010003

Chen Z, Shatara S, Tan X (2010) Modeling of biomimetic robotic fish propelled by an ionic polymer–metal composite caudal fin. IEEE/ASME Trans Mechatron 15(3):448–459

Cox WC, Simpson JA, Domizioli CP, Muth JF, Hughes BL (2008) An underwater optical communication system implementing Reed-Solomon channel coding. In: Proceedings of 2008 OCEANS conference. Boston, MA, pp 1–6

Cui Y, Sarkar N (2000) A unified force control approach to autonomous underwater manipulation. In: Proceedings 2000 IEEE international conference on robotics and automation (ICRA 2000). pp 255–266

De Novi G, Melchiorri C, Garcia JC, Sanz PJ, Ridao P, Oliver G (2009) A new approach for a reconfigurable autonomous underwater vehicle for intervention. In: Systems conference, 2009 3rd annual IEEE. pp 23–26

Dudek G, Giguere P, Prahacs C, Saunderson S, Sattar J, Torres-Mendez L, Jenkin M, German A, Hogue A, Ripsman A, Zacher J, Milios E, Liu H, Zhang P, Buehler M, Georgiades C (2007) AQUA: an amphibious autonomous robot. Computer 40(1):46–53

Gao B, Guo S (2010) Development of an infrared sensor-based wireless intelligent fish-like underwater microrobot. In: Proceedings of 2010 IEEE international conference on information and automation. Harbin, pp 1314–1318. 20–23 June 2010

Gao B, Guo S, Ye X (2011) Motion-control analysis of ICPF-actuated underwater biomimetic microrobots. Int. J. Mechatron Autom 1(2):79–89

Jun B, Lee P, Kim S (2008) Manipulability analysis of underwater robotic arms on ROV and application to task-oriented joint configuration. J Mech Sci Technol 22:887–894

Kim HJ (2011) Smart soft-morphing structure: design, manufacturing, and application. Ph.D. Thesis, School of Mechanical and Aerospace Engineering, Seoul National University

Li M, Guo S, Hirata H, Ishihara H (2015) Design and performance evaluation of an amphibious spherical robot. Robot Auton Syst 64:21–34. doi:10.1016/j.robot.2014.11.007

Lin X, Guo S, Tanaka K, Hata S (2010) Development and evaluation of a vectored water-jet-based spherical underwater vehicle. Inf Int Interdiscip J 13(6):1985–1998

Marani G, Choi S, Yuh J (2009) Underwater autonomous manipulation for intervention missions AUVs. Ocean Eng 36:15–23

Mohan S, Kim J (2012) Indirect adaptive control of an autonomous underwater vehicle–manipulator system for underwater manipulation tasks. Ocean Eng 54:233–243

Mohan S, Kim J (2015) Coordinated motion control in task space of an autonomous underwater vehicle–manipulator system. Ocean Eng 104:155–167

Shi L, Guo S, Li M, Mao S, Xiao N, Gao B, Song Z, Asaka K (2012) A novel soft biomimetic microrobot with two motion attitudes. Sensors 12(12):16732–16758

Tian B, Zhang F, Tan X (2013) Design and development of an LED-based optical communication system for autonomous underwater robots. In: Proceedings of 2013 IEEE/ASME international conference on advanced intelligent mechatronics, pp 1558–1563

Toshiba 4-legged nuclear plant inspection robot (2012) (Online). http://www.exponentialtimes.net/videos/toshiba-4-legged-nuclear-plant-inspection-robot/

Yeom SW, Oh IK (2009) A biomimetic jellyfish robot based on ionic polymer metal composite actuators. Smart Mater Struct 18, Paper No. 085002

Yu SC, Yuh J, Kim J (2013) Armless underwater manipulation using a small deployable agent vehicle connected by a smart cable. In: Ocean engineering. pp 149–159

Yue C, Guo S, Shi L (2015) Design and performance evaluation of a biomimetic microrobot for the father–son underwater intervention robotic system. Microsyst Technol. doi:10.1007/s00542-015-2457-z

Zhang S, Liang X, Xu L, Xu M (2013) Initial development of a novel amphibious robot with transformable fin-leg composite propulsion mechanisms. J Bionic Eng 10(4):434–445